Validation of a vector version of the 6S radiative transfer code for atmospheric correction of satellite data. Part II. Homogeneous Lambertian and anisotropic surfaces

Svetlana Y. Kotchenova* and Eric F. Vermote

Department of Geography, University of Maryland, 4321 Hartwick Road, Suite 209, College Park, Maryland 20740

*Corresponding author: skotchen@ltdri.org

Received 20 December 2006; revised 2 March 2007; accepted 5 March 2007;
posted 13 March 2007 (Doc. ID 78252); published 20 June 2007

This is the second part of the validation effort of the recently developed vector version of the 6S (Second Simulation of a Satellite Signal in the Solar Spectrum) radiative transfer code (6SV1), primarily used for the calculation of look-up tables in the Moderate Resolution Imaging Spectroradiometer (MODIS) atmospheric correction algorithm. The 6SV1 code was tested against a Monte Carlo code and Coulson's tabulated values for molecular and aerosol atmospheres bounded by different Lambertian and anisotropic surfaces. The code was also tested in scalar mode against the scalar code SHARM to resolve the previous 6S accuracy issues in the case of an anisotropic surface. All test cases were characterized by good agreement between the 6SV1 and the other codes: The overall relative error did not exceed 0.8%. The study also showed that ignoring the effects of radiation polarization in the atmosphere led to large errors in the simulated top-of-atmosphere reflectances: The maximum observed error was approximately 7.2% for both Lambertian and anisotropic surfaces.

OCIS codes: 280.1310, 290.4210, 010.1300, 010.1310, 010.1320, 120.0280.

1. Introduction

This paper describes the second part of the validation effort of a vector version of the 6S (Second Simulation of a Satellite Signal in the Solar Spectrum) radiative transfer (RT) code. The first part of the validation was devoted to the testing of 6S against other RT codes and valuable benchmarks for different molecular, aerosol, and mixed atmospheres, bounded by black soil [1]. The second part will include the influence of different homogeneous Lambertian and anisotropic surfaces.

The 6S code is a basic code underlying the Moderate Resolution Imaging Spectroradiometer (MODIS) atmospheric correction algorithm [2]. Its first vector version (6SV1.0B, hereinafter simply referred to as 6SV1), which accounts for the polarization of solar radiation in the atmosphere, was publicly released in May 2005, and can be downloaded from http://www.6s.ltdri.org. This Web site also contains a link to a special interface for the creation of 6SV1 input files and information on all recent updates.

The 6SV1 code is based on the vector method of successive orders of scattering (SOS) approximations [3], which was incorporated into the code by Vermote. The effects of polarization are accounted for through the calculation of the Q and U components of the Stokes vector, $\vec{I} = \{I, Q, U, V\}$, which describe the degree and plane of polarization of electromagnetic radiation [4]. The code works under the assumption of linearly polarized light, i.e., the component V, characterizing the ellipticity of polarization, is set to 0. A detailed description of the new features incorporated into 6SV1 along with light polarization can be found in the 6S manual [5] and the Part I validation study [1].

Ground surface modeling in 6SV1 includes simulations of homogeneous surfaces with or without a directional effect (dependence of the direction of reflected light on the direction of incident light) and nonhomogeneous surfaces. The modeling of a homogeneous surface with no directional effect includes constant as well as wavelength-dependent Lamber-

0003-6935/07/204455-10$15.00/0

tian surfaces and the choice of four standard uniform surfaces. To account for the bidirectional effect, the users are provided with a set of ten different bidirectional reflectance distribution function (BRDF) models and the option to input their own BRDF values.

In addition to its own elaborate validation process, 6SV1 is participating in a joint vector/scalar RT code comparison project performed by the MODIS Atmospheric Correction Group in collaboration with the NASA Goddard Space Flight Center. Within this project, the performances of 6SV1 and several other commonly used RT codes, such as vector/scalar RT3 [6], Vector Program Dave (VPD) [7,8], and scalar SHARM [9], are evaluated based on comparisons with standard benchmark approaches. All information about this project, including the descriptions of the codes, conditions, and results of the comparison, is posted at http://www.rtcodes.ltdri.org. The scalar codes have been included to perform a standard evaluation of the effects of polarization under given comparison conditions.

The creation of 6SV1, along with its validation and testing against other RT codes, was inspired by numerous studies demonstrating the significance of the effects of polarization [10–12]. The comparison between vector and scalar top-of-atmosphere (TOA) reflectances, presented in the Part I validation study [1], also confirmed the strong influence of polarization. The relative error of scalar simulations was more than 10% for a molecular atmosphere, reached 5% for an aerosol atmosphere, and varied within 6% for a mixed (aerosol + molecular) atmosphere.

2. Validation Scheme

The code comparison scheme for the Part II validation study is presented in Fig. 1. 6SV1 has been run in vector (with polarization) and scalar (without polarization) modes. The scalar mode is enabled by putting the polarization index and depolarization factor to 0. The polarization index controls the calculation of the Stokes vector components Q and U. The depolarization factor accounts for the deviation of a particle shape from a symmetrical sphere owing to the presence of a radiation field [4].

Scalar mode calculations were included in this part of the study only to resolve the previous 6S accuracy issues [13]. In scalar mode, the performance of 6SV1 was evaluated against the scalar code SHARM for Lambertian and anisotropic surfaces. The anisotropic surface was simulated with the help of the RPV model developed by Rahman *et al*. [14].

In vector mode, the performance of 6SV1 was evaluated against two standard benchmarks: Coulson's tabulated values [15] for a Lambertian surface and a Monte Carlo code [16] for Lambertian and anisotropic surfaces. The anisotropic surface in this case was presented by the RPV model [14] and the Roujean *et al*. BRDF model [17].

The effects of polarization were estimated through the comparison of TOA reflectances calculated by 6SV1 in scalar and vector modes for Lambertian and ocean surfaces.

3. 6SV1 BRDF Models Used in the Study

The RPV model is a semiempirical model simulating the BRDF of arbitrary natural surfaces in the visible and near-infrared spectra [14]. The model requires the input of three independent parameters: the arbitrary parameter ρ_0 characterizing the intensity of the reflectance of a surface, the asymmetry parameter Θ controlling the relative amount of forward and backward scattering, and the structural parameter k defining the level of anisotropy of the surface. It successfully reproduces the field-measured reflectances of a number of different surfaces ranging from bare soil to full canopy cover. In this study, this model is used to simulate grass surface and shrubs using the best-fit parameters extracted from Engelsen *et al*. [18] (see Table 1).

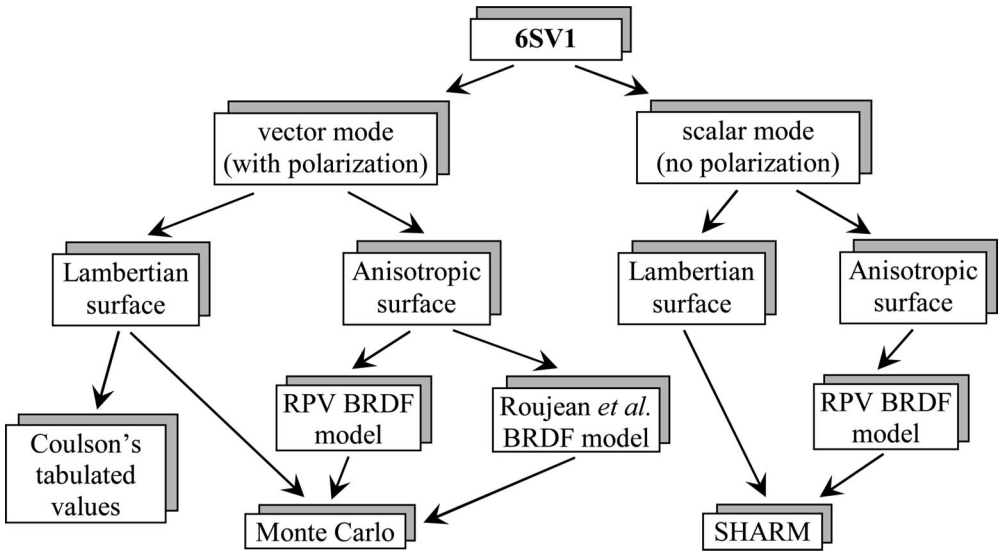

Fig. 1. Part II validation scheme.

Table 1. Parameters of the 6SV1 BRDF Models used in the Part II Validation Study

Model	Parameters	Description of Parameters	Simulated Surfaces	
RPV	ρ_0	Intensity of the reflectance of the surface	0.032	0.242
	Θ	Asymmetry parameter of the scattering phase function	−0.073	−0.032
	k	Level of anisotropy of the surface	1.047 (Shrubs)	0.637 (Grass)
Roujean *et al*.	k_0	Surface parameter (bidirectional reflectance at nadir)	0.037	
	k_1	Surface parameter (diffuse reflection by opaque objects)	0.0	
	k_2	Surface parameter (volume scattering)	0.133 (Pine forest)	
Ocean	w_s	Wind speed, m/s	11.0	
	φ_w	Wind direction (°)	30.0	
	C_{sal}	Salt concentration, ppt	35.0	
	C	Pigment concentration, mg/m^3	0.3	

The Roujean *et al*. surface model is also a semiempirical BRDF model designed to be applicable to heterogeneous surfaces [17]. It operates on the basis of three input surface parameters (k_0, k_1, and k_2), which are related to basic macroscopic properties of a particular surface (see Table 1). The surface BRDF is calculated as a combination of reflectances resulting from two major processes: diffuse reflection by material objects, which accounts for the geometrical structure of opaque reflectors and shadowing effects, and volume scattering by a collection of dispersed facets, which accounts for scattering properties of leaf elements. The first process is described using a model of vertical opaque protrusions reflecting in accordance with the Lambert law, while the second process is described on the basis of a simple RT theory. This model also serves as a prototype for a linear kernel-driven MODIS BRDF model underlying the operational MODIS BRDF/albedo algorithm [19,20]. In this study, the model is filled with pine forest parameters experimentally obtained by Kimes *et al*. [21].

The ocean BRDF model adopted in 6SV1 assumes that the directional reflectance of an ocean surface is composed of three components: reflection of foam (or whitecaps) [22], specular reflection [23–27], and reflection attributable to underlight (the scattering of radiation by water molecules and suspended material in the water) [28]. The current 6SV1 ocean model requires the input of four independent parameters: the wind speed w_s in m/s, direction of the wind φ_w in degrees (measured clockwise from the North), salt concentration C_{sal} in ppt, and pigment concentration C (Chl a + Pheo a) in mg/m^3. The values of these parameters, listed in Table 1, were selected based on the results of extensive literature and Internet searching [29–31].

A brief mathematical descriptions of these three models, together with corresponding references, are provided in the Appendixes. We believe that the use of a Lambertian surface and three different BRDF models in this validation study will be satisfactory to draw a general conclusion on the performance of 6SV1.

4. Performance of 6S in Scalar Mode (Testing Against SHARM)

The results of the previous comparison study with the scalar code SHARM (developed by Lyapustin), which are of interest here, include simulations for two pure aerosol atmospheres bounded by a grass surface in the NIR spectral region (wavelength $\lambda = 0.750$ μm) [13]. Both NIR Clear (aerosol optical thickness $\tau_{aer} = 0.2$) and NIR Hazy ($\tau_{aer} = 0.8$) aerosol atmospheres were represented by a regular continental aerosol model requiring 128 Legendre coefficients for its accurate simulation. The grass surface was represented by the RPV model [14] with the parameters specified in Table 1. The average relative error of scalar 6S TOA simulated reflectances, calculated using SHARM as a reference, was found to be in the range of 4%–6% for both cases.

Our suggestion is that such disagreement was associated with both atmospheric and surface modeling. First, it was not possible to vary the number of Legendre coefficients used for the description of a phase function in the previous scalar 6S. This number was fixed to 81 (83 angles, including 0° and 180°). As a result, the comparison was done using 128 Legendre coefficients for SHARM and other RT codes and only 81 coefficients for 6S, letting an error in the phase function modeling lead to a further error in TOA reflectances. (It should be noted here that in all versions of 6S the number of Legendre coefficients is strictly responsible for the accuracy of aerosol phase function modeling, while in SHARM this number is defined as the number of spherical harmonics and is responsible for the accuracy of RT simulations.) Second, in the previous scalar 6S the influence of anisotropic surface was incorporated into the RT body of the code using approximate empirical formulas [5].

The first suggestion has been thoroughly checked in the Part I validation study [1]. The released 6SV1 code provides the user with an opportunity to arbitrarily change the number of Legendre coefficients. Using this option, we compared 6SV1 in scalar mode to DISORT,

which was stated to have excellent agreement with SHARM [13], at $\lambda = 0.694$ μm for three values of $\tau_{aer} = \{0.2; 0.78; 2.0\}$ and a more complex continental aerosol model characterized by a phase function with 220 Legendre coefficients. The scalar 6S and DISORT TOA reflectances agreed within 0.15% for view zenith angle (VZA) below 70° for all three values of τ_{aer}; the disagreement became slightly worse (within 0.27%) for VZA above 70° for $\tau_{aer} = 2.0$.

The second suggestion has been verified in this part of the study. We compared TOA reflectances calculated by SHARM and 6SV1 in scalar mode for the following conditions: the standard continental aerosol model used in Part I, $\tau_{aer} = \{0.2, 0.8\}$, $\lambda = 750$ nm, AZ (relative azimuth) = {0°, 90°, 180°}, VZA = {0°–79°}, solar zenith angle (SZA) = {0.0°, 10.0°, 23.07°, 45.0°, 58.67°, 75.0°}, and three types of boundary surface: (a) Lambertian with $\rho = 0.25$, (b) the RPV grass model incorporated into the RT body of the code using the approximate formulas, and (c) the RPV grass model incorporated directly in the lower boundary condition as a Fourier-series expansion of the reflection matrix in accordance with the technique outlined in Deuzé *et al*. [3].

Figure 2 illustrates the results. There is excellent agreement between the reflectances calculated by SHARM and 6SV1 in scalar mode for the Lambertian surface [see Fig. 2(a)]. The relative difference varies from −0.01% to 0.16%. The agreement is much worse for the case of indirectly incorporated BRDF. The relative error calculated using 6SV1 scalar simulations as references oscillates from −0.9% to 5.0% for $\tau = 0.2$

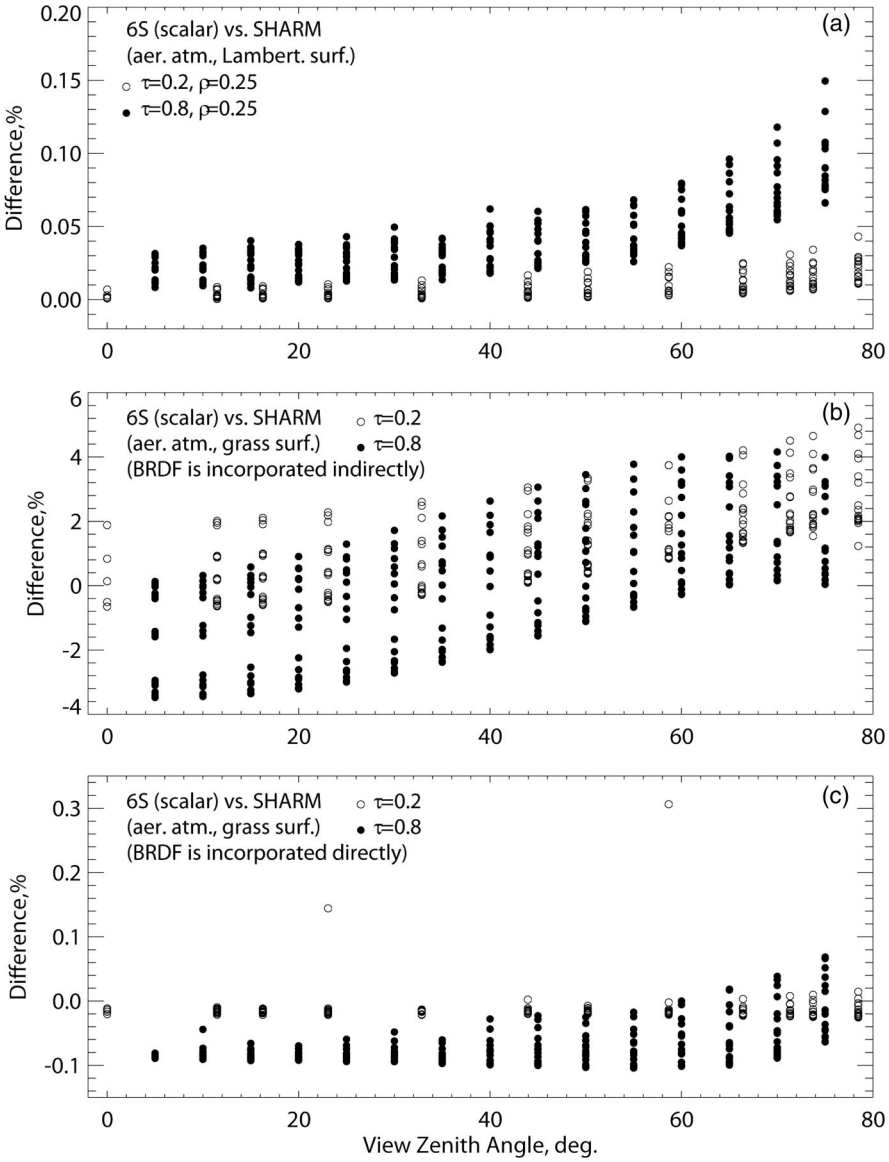

Fig. 2. Validation of 6SV1 in scalar mode against SHARM for Lambertian and anisotropic surfaces. For all three plots the aerosol atmosphere is presented by the standard continental model, $\tau_{aer} = \{0.2; 0.8\}$, $\lambda = 750$ nm, SZA = {0.0°, 10.0°, 23.07°, 45.0°, 58.67°, 75.0°}, AZ = {0°, 90°, 180°}, and VZA = {0°–79°}. (a) Lambertian surface with the ground reflectance $\rho = 0.25$, (b) RPV grass model incorporated into the code through the approximate formulas, and (c) the same model incorporated directly.

and from −4.0% to 4.4% for $\tau = 0.8$ [see Fig. 2(b)], in consistency with the results reported in the previous comparison study [13]. All this error seems to be induced by the approximate formulas for the incorporation of surface influence since the 6SV1 scalar simulations with the directly incorporated BRDF demonstrate excellent agreement with SHARM [see Fig. 2(c)]. The absolute value of relative difference stays within 0.11% for both values of optical thicknesses, except for a couple of points for $\tau_{aer} = 0.2$, where the upper boundary limit is 0.15% and 0.31%.

The β version of 6SV1, released in May, 2005, still uses the approximate formulas for the incorporation of surface influence. However, the next vector version of 6S (6SV2), which is planned to be released in the near future, will operate based on the direct incorporation of BRDF simulations.

5. Performance of 6S in Vector Mode

A. Validation Against Coulson's Tabulated Values

Coulson's tabulated values represent the accurate calculations of the solar radiation reflected and transmitted by a plane-parallel, nonabsorbing molecular atmosphere in accordance with Rayleigh's law [15]. They are generally considered a benchmark for verification of the accuracy of a vector RT code [6,32].

The comparison between 6SV1 and Coulson's reflectances was performed for four different sets of parameters: (1) $\tau_{mol} = 0.1$, $\rho = 0.25$, SZA = {0.0°, 36.87°, 66.42°}; (2) $\tau_{mol} = 0.1$, $\rho = 0.8$, SZA = {23.07°, 53.13°, 78.46°}; (3) $\tau_{mol} = 0.25$, $\rho = 0.25$, SZA = {23.07°, 53.13°, 78.46°}; and (4) $\tau_{mol} = 0.25$, $\rho = 0.8$, SZA = {0.0°, 36.87°, 66.42°}, where τ_{mol} is the optical thickness of a molecular atmosphere, and ρ is the reflectance of a bounding Lambertian surface. Six values of VZA from 0° to 79° and three values of AZ = {0°, 90°, 180°} were selected for each set of parameters. The optical thicknesses of 0.1 and 0.25 approximately correspond to the wavelengths of 0.530 and 0.440 μm, according to the computations of 6SV1.

Figure 3 illustrates the results. We plotted the absolute values of relative differences between Coulson and 6SV1 TOA reflectances, calculated using Coulson's values as references. Excellent agreement is observed for all sets of parameters, which establishes the general accuracy of 6SV1 simulations in the case of a molecular atmosphere at 0.1%.

Coulson's tabulated values also include calculations of the other Stokes vector components, such as Q and U. However, an intensive comparison between 6SV1 and Coulson's Q and U parameters was presented in the Part I validation study [1] and does not need to be repeated here as the main goal of this part is to validate the code for cases involving the reflection from different Lambertian and anisotropic surfaces.

B. Validation Against Monte Carlo

The Monte Carlo code used in this study is a 3D forward RT model created on the basis of the four-component Stokes vector approach. The code was primarily developed by Bréon [16] for atmosphere–ocean interaction studies and modified later by the MODIS Atmospheric Correction Group. A short description of the code is provided in the Part I validation study [1]. A Monte Carlo approach is often considered by the scientific community one of the most accurate ways to generate benchmark values [33,34] as it has no other limitations except a large amount of calculation time and angular space discretization.

The Lambertian, RPV BRDF [14] and the Roujean *et al*. BRDF [17] surface models are not included in the original version of the code. They were later incorporated into the code for the purposes of this study. Also, a special method was applied to integrate 6S TOA reflectances over the output solid angles of Monte Carlo [1].

The results of the comparison between 6SV1 and Monte Carlo are presented in Figs. 4(a) and 4(b) for Lambertian surfaces and in Fig. 4(c) for different anisotropic surfaces. All plots are drawn in polar coordinates. The specified angular coordinates designate the boundary VZA values for the sampling of the VZA range (from 0° to 90°) at the top of atmosphere. The relative AZ space (from 0° to 180°) is divided into eight

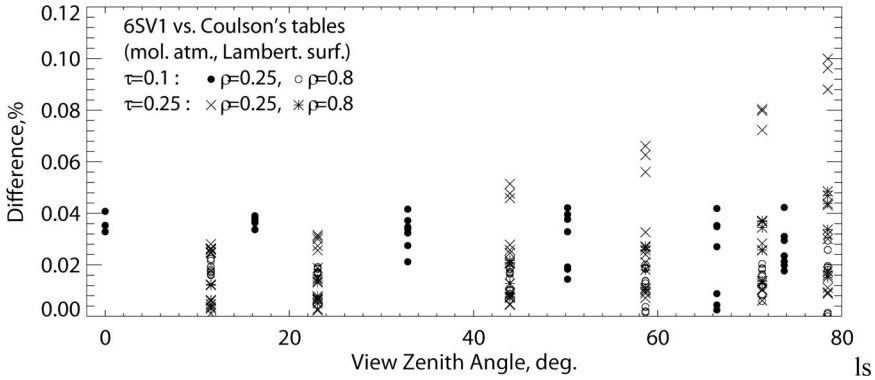

Fig. 3. Validation of 6SV1 against Coulson's tabulated values for a molecular atmosphere bounded by a Lambertian surface. The validation was performed for four different cases: (1) $\tau_{mol} = 0.1$, $\rho = 0.25$, SZA = {0.0°, 36.87°, 66.42°}; (2) $\tau_{mol} = 0.1$, $\rho = 0.8$, SZA = {23.07°, 53.13°, 78.46°}; (3) $\tau_{mol} = 0.25$, $\rho = 0.25$, SZA = {23.07°, 53.13°, 78.46°}; and (4) $\tau_{mol} = 0.25$, $\rho = 0.8$, SZA = {0.0°, 36.87°, 66.42°}.

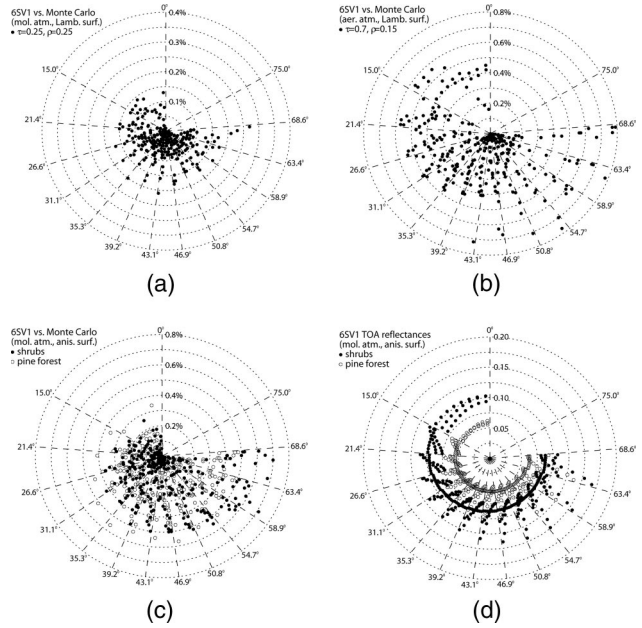

Fig. 4. (a) Validation of 6SV1 against Monte Carlo for a molecular atmosphere ($\tau_{mol} = 0.25$) bounded by a Lambertian surface ($\rho = 0.25$). The specified angular coordinates designate the boundary VZA values for the Monte Carlo output solid angles. The radius coordinate designates the relative difference between the TOA reflectances of both codes. SZA = {0.0°; 23.0°; 50.0°}. (b) Validation of 6SV1 against Monte Carlo for a clean maritime aerosol atmosphere ($\tau_{aer} = 0.7$) bounded by a Lambertian surface ($\rho = 0.15$). The geometrical conditions are the same as in (a). The simulations were performed at $\lambda = 0.550$ μm. (c) Validation of 6SV1 against Monte Carlo for a molecular atmosphere with $\tau_{mol} = 0.093$ bounded by shrubs (the RPV BRDF model [14], filled circles) and for a molecular atmosphere with $\tau_{mol} = 0.054$ bounded by pine forest (the Roujean *et al*. BRDF model [17], open circles). The geometrical conditions are the same as in (a). (d) TOA reflectances calculated by 6SV1 for a molecular atmosphere with $\tau_{mol} = 0.093$ bounded by shrubs (the RPV BRDF model, filled circles) and for a molecular atmosphere with $\tau_{mol} = 0.054$ bounded by pine forest (the Roujean *et al*. BRDF model, open circles). The geometrical conditions are the same as in (a).

equal angles of 22.5° each. The relative difference between the outputs of the codes, calculated using Monte Carlo as a reference, is presented by the radius coordinate. The SZA values are the same as in the Part I validation study, i.e., SZA = {0.0°, 23.0°, 50.0°}. 1×10^{10} photons are sufficient to establish the average accuracy of the Monte Carlo code below 0.24% in the case of a molecular atmosphere. This number usually has to be increased to 3×10^{10} for calculations involving an aerosol atmosphere.

Figure 4(a) shows the results of simulations for a molecular atmosphere ($\tau_{mol} = 0.25$) bounded by a Lambertian surface with $\rho = 0.25$. This case is characterized by very good agreement between the 6SV1 and Monte Carlo TOA reflectances. The relative difference stays within 0.3% for VZA < 68.6° and slightly increases up to 0.4% for VZA from 68.6° to 75.0°.

Figure 4(b) illustrates the results for a hazy aerosol atmosphere ($\tau_{aer} = 0.7$) bounded by a Lambertian surface with $\rho = 0.15$. The atmosphere is represented by the clean maritime aerosol model used in the Part I validation study [1], composed of biogenically produced sulfate and sea-salt particles in nuclei and accumulation modes [35]. The simulations were performed for $\lambda = 0.550$ μm. This case also shows good agreement between the outputs of the two codes. The maximum observed absolute value of relative error is equal to 0.79% for VZA > 63.4°. Below VZA = 54.7° the relative error varies within 0.6%. The error seems to increase slightly for backscattering calculations for all SZA values, compared to forward scattering.

The results of simulations for a molecular atmosphere bounded by shrubs and pine forest are presented in Fig. 4(c). The shrubs were simulated by the RPV model [14], while the pine forest was created on the basis of the Roujean *et al*. model [17]. The parameters for both surfaces are listed in Table 1. For the RPV model the simulations were performed at $\lambda = 0.550$ μm (green spectrum, $\tau_{mol} = 0.093$), while for the Roujean *et al*. model the simulations were done at $\lambda = 0.630$ μm (red spectrum, $\tau_{mol} = 0.054$). Both cases are characterized by good agreement between the 6SV1 and Monte Carlo TOA reflectances. The relative error stays within 0.6% for the shrubs and does not exceed 0.71% for the pine forest.

The actual TOA reflectances calculated by 6SV1 for both the shrub and pine forest cases are shown in Fig. 4(d). The reflectance of shrubs is slightly higher than that of pine forest as they constitute a brighter surface in the visible spectrum.

6. Effects of Polarization

The effects of polarization will be demonstrated through the comparison of TOA reflectances calculated by 6SV1 in vector and scalar modes. To reproduce real measurement conditions of passive satellites as close as possible, the simulations were done using two MODIS spectral bands and AERONET data collected over Midway Islands.

The Midway Islands is a coral atoll in the Pacific Ocean located approximately 2334 km northwest of Honolulu near the end of the Hawaiian Archipelago (28.12 °N, 177.22 °W) [36]. It is characterized by a subtropical climate with cool, moist winters (December to February) and warm, dry summers (May to October), moderated by prevailing easterly winds. Most of its 42 inches of annual rainfall occurs during the winter.

The Midway Islands AERONET data set used in this study for modeling an aerosol atmosphere was collected on 31 January 2002. The set includes an average size distribution of particles, illustrated in Fig. 5(a), and values of refractive indices at four different wavelengths, which were linearly extrapolated and interpolated between the 6SV1 node wavelengths. The aerosol was slightly absorbing, with the single scattering albedo (SSA) of 0.987, as calculated in 6SV1. A molecular atmosphere was accepted as modeled in 6SV1 on the basis of the standard US62 pattern parameters, an exponential

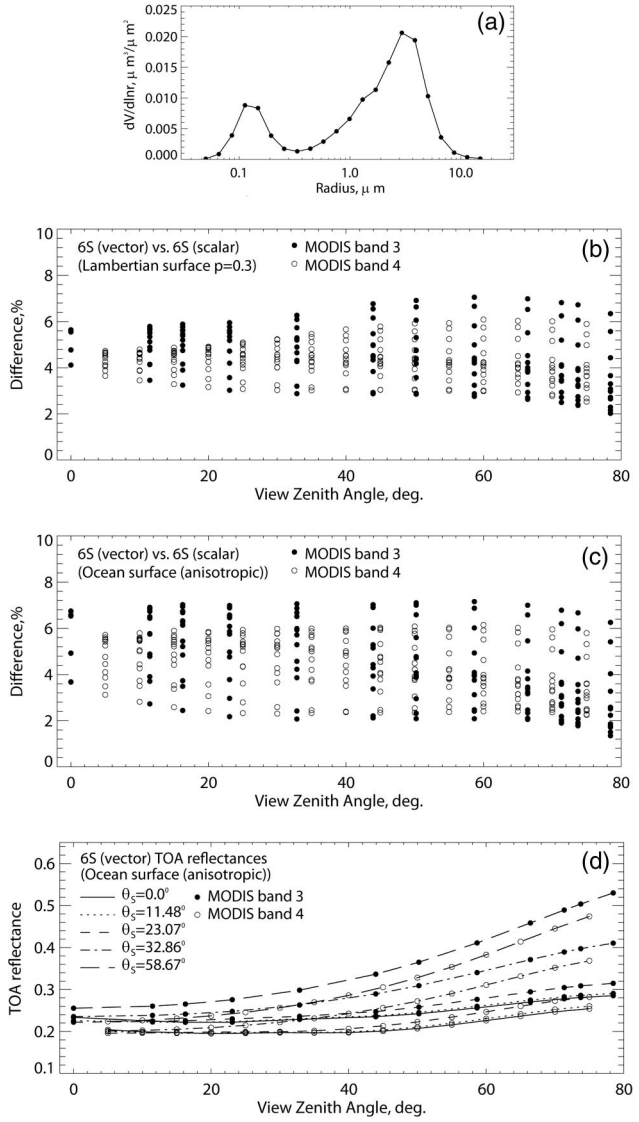

Fig. 5. (a) Average volume size distribution of aerosol particles measured by AERONET over Midway Islands (28.12 °N, 177.22 °W) on 31 January 2002. (b)–(c) Effects of polarization for a mixed (molecular + aerosol) atmosphere bounded by a Lambertian surface with (b) the ground reflectance $\rho = 0.3$ (b) and (c) an ocean surface. The aerosol constituent is modeled using the Midway Islands size distribution shown in (a). SZA = {0.0°, 10.0°, 23.07°, 45.0°, 58.67°, 75.0°}; AZ = {0°, 90°, 180°}; VZA = {0°–79°}. The ocean surface model parameters are specified in Table 1. The optical thickness values are listed in Table 2. (d) 6SV1 TOA reflectances for the mixed atmosphere bounded by the ocean surface. SZA (designated by θ_S) = {0.0°, 10.0°, 23.07°, 45.0°, 58.67°}; AZ = 90°; VZA = {0°–79°}. The ocean surface model parameters are specified in Table 1. The optical thickness values are listed in Table 2.

vertical profile and the maximum height of 8 km. The molecular and aerosol constituents were mixed using simple proportion formulas [1]. The optical thicknesses of molecular, aerosol, and mixed (molecular + aerosol) atmospheres are listed in Table 2 for both scalar and vector cases.

The two MODIS bands used for the comparison cover the blue (band 3, 0.459–0.479 nm) and green

Table 2. Optical Thicknesses of Molecular, Aerosol, and Mixed (Molecular + Aerosol) Atmospheres[a]

		Optical Depth		
Mode	MODIS Band	Rayleigh	Aerosol	Mixed
Scalar	3	0.18377	1.63105	1.81482
	4	0.90750	1.49514	1.58589
Vector	3	0.19260	1.63105	1.82365
	4	0.09511	1.49514	1.59025

[a]Optical thicknesses over Midway Islands calculated by 6SV1 in vector and scalar modes for MODIS bands 3 and 4 on the basis of the US62 standard molecular atmosphere parameters and AERONET data collected on 31 January 2002.

(band 4, 0.545–0.565 nm) MODIS spectral ranges. The selected geometrical conditions, SZA = {0.0°, 10.0°, 23.07°, 45.0°, 58.67°, 75.0°}, AZ = {0°, 90°, 180°}, and VZA = {0°–79°}, cover a wide range of possible angular configurations. The ground boundary conditions were simulated as a Lambertian surface with $\rho = 0.3$ and an anisotropic ocean surface[5] with the parameters listed in Table 1.

The results of the comparison are presented in Fig. 5(b) for the Lambertian surface and in Fig. 5(c) for the ocean surface. The plots show the relative scalar TOA reflectance errors calculated using the following formula: [(vector-scalar)/vector]*100%. Band 3 is characterized by larger errors of the scalar mode in both cases owing to the more significant contribution of molecular scattering in the blue spectrum. Its error range is spread between approximately 1.4% and 7.2%, while for band 4 the error varies within 6.2%. In all cases, ignoring the influence of polarization leads to a significant underestimation (up to 7.2%) of TOA reflectances. The error becomes larger for the backscattering direction, which is specified as AZ = 0° in 6SV1.

The TOA reflectances calculated for the ocean surface case by 6SV1 in vector mode are shown in Fig. 5(d). We plotted the reflectances for AZ = 90° and the first five values of SZA. As expected, the simulated reflectances are larger for the MODIS blue band.

6SV1 works a little slower than its scalar predecessor. To demonstrate this we performed test scalar and vector calculations for one of the cases considered in this section: the Midway Islands atmosphere,

Table 3. Example of Time Estimates[a] for Scalar and Vector Calculations Depending on the Number of Legendre Coefficients[b]

	Time, Seconds Legendre Coefficients			
Mode of 6SV1	83 (Default)	123	153	203
Vector	4.93 (3.85)	7.24 (5.62)	8.81 (6.65)	11.20 (8.20)
Scalar	2.39 (1.13)	3.06 (1.35)	3.71 (1.52)	4.42 (1.69)

[a]The calculations were performed on Pentium 4 CPU 2.80 Ghz.
[b]6SV1 is run in vector and scalar modes to simulate TOA reflectance measured by MODIS band 3 over Midway Islands. The values in the parentheses show how much time is required when the precomputed aerosol model is read from a file [5].

MODIS band 3, Lambertian ground with $\rho = 0.3$ SZA = 10°, AZ = 90°, VZA = 30°. Example amounts of time required for the calculations are listed in Table 3. It should be noted, however, that these estimates are true only for this particular case, as the speed of 6SV1 depends not only on the number of Legendre coefficients [1] but also on the selected aerosol model, geometry, and accuracy of RT simulations.

7. Conclusions

The study presented in this paper completes the validation effort of the recently developed vector version of the 6S RT code (6SV1). The obtained results confirm the good performance of the code over homogeneous Lambertian and anisotropic surfaces. The TOA reflectances calculated by 6SV1 for different molecular atmospheres bounded by Lambertian surfaces agree within 0.11% with the values extracted from Coulson's tables and within 0.4% with those calculated by the Monte Carlo code. The substitution of a molecular atmosphere by an aerosol composition leads to an insignificant decrease of agreement: The relative error fluctuates within 0.8% in comparison with Monte Carlo. The use of anisotropic surfaces instead of Lambertian ones also provides very good agreement between the 6SV1 and Monte Carlo outputs: The relative difference stays within 0.6% for the Roujean *et al*. model and does not exceed 0.71% for the RPV BRDF model.

The previous 6S accuracy issues have been totally resolved. We incorporated the treatment of surface BRDF in the SOS module of the code directly as ground boundary conditions, and its accuracy (versus SHARM) improved by an order of magnitude compared to the previously used approximation. The direct incorporation of BRDF will be included in the next vector version of 6S (6SV2), which is planned to be released in the near future.

The polarization of radiation in the atmosphere has been shown to have significant influence on calculated TOA reflectances in the case of both Lambertian and anisotropic (ocean) surfaces. Ignoring the effects of polarization led to the presence of a large relative error (up to 7.2%) in scalar simulations. This error significantly increases the standard RT code accuracy requirement of 1.0%.

Unfortunately, it was not possible to estimate the effects of surface polarization. Despite its ability to accurately simulate the polarization of radiation in the atmosphere, 6SV1 still works under the assumption that the underlying ground surface is not polarized. Moreover, none of the other publicly available RT codes incorporates a surface polarization model. The inclusion of one will be our next step in the further development of the vector 6S.

We also plan to continue working on the joint code comparison project, which will define the position of 6SV1 among other RT codes used in the remote sensing community. Currently, 6SV1 is gradually replacing its previous scalar predecessor for the calculation of look-up tables in the MODIS atmospheric correction algorithm. Collection 5 of MODIS surface reflectances is being produced using 6SV1. We also encourage all users of the code to switch to its vector version. Information on further updates of the vector 6S can always be found on the code Web site.

Appendix A. RPV BRDF Model

The reflectance ρ_s of an arbitrary natural surface is simulated as [14]

$$\rho_s(\theta_s,\ \phi_s,\ \theta_v,\ \phi_v) = \rho_0 \frac{\cos^{k-1}\theta_s \cos^{k-1}\theta_v}{(\cos\theta_s + \cos\theta_v)^{1-k}} F(\xi)[1 + R(G)], \tag{A1}$$

where θ_s and ϕ_s are solar zenith and azimuth angles, θ_v and ϕ_v are view zenith and azimuth angles, ρ_0 is the arbitrary parameter characterizing the intensity of the reflectance of the surface cover, k is the parameter indicating the level of anisotropy of the surface, G is the geometrical factor given by

$$G = \left[\tan^2\theta_s + \tan^2\theta_v - 2\tan\theta_s \tan\theta_v \cos(\phi_s - \phi_v)\right]^{1/2}, \tag{A2}$$

$F(\xi)$ is the modified Henyey and Greenstein function defined as

$$F(\xi) = \frac{1 - \Theta^2}{\left[1 + \Theta^2 - 2\Theta\cos(\pi - \xi)\right]^{1.5}}, \tag{A3}$$

with the phase angle ξ given by

$$\cos\xi = \cos\theta_s \cos\theta_v + \sin\theta_s \sin\theta_v \cos(\phi_s - \phi_v), \tag{A4}$$

and the asymmetry factor Θ controlling the relative amount of forward ($0 \le \Theta \le +1$) and backward ($-1 \le \Theta \le 0$) scattering, and R(G) is the function accounting for the hot-spot effect, defined as

$$R(G) = \frac{1 - \rho_0}{1 + G}. \tag{A5}$$

Appendix B. Roujean BRDF Model

The bidirectional reflectance of a surface is calculated as [17]

$$\rho(\theta_s,\ \theta_v,\ \phi) = k_0 + k_1 f_1(\theta_s,\ \theta_v,\ \phi) + k_2 f_2(\theta_s,\ \theta_v,\ \phi), \tag{B1}$$

where θ_s and θ_v are solar and view zenith angles, $\phi = \phi_s - \phi_v$ is the relative azimuth (ϕ_s and ϕ_v are solar and view azimuth angles), k_0, k_1, and k_2 are parameters related to basic macroscopic properties of a surface, f_1 is an analytical function simulating diffuse reflection of opaque rectangular protrusions placed on a horizontal surface:

$$f_1(\theta_s,\ \theta_v,\ \phi) = \frac{1}{2\pi}\{(\pi - \phi)\cos(\phi) + \sin(\phi)\}\tan(\theta_s)\tan(\theta_v) - \frac{1}{\pi}\{\tan(\theta_s) + \tan(\theta_v) + \sqrt{\tan^2(\theta_s) + \tan^2(\theta_v) - 2\tan(\theta_s)\tan(\theta_v)\cos(\phi)}\}, \quad \text{(B2)}$$

and f_2 is an analytical function simulating the volume scattering of dispersed facets (leaf elements):

$$f_2(\theta_s,\ \theta_v,\ \phi) = \frac{4}{3\pi}\frac{1}{\cos(\theta_s) + \cos(\theta_v)}\left\{\left(\frac{\pi}{2} - \xi\right) \times \cos(\xi) + \sin(\xi)\right\} - \frac{1}{3}, \quad \text{(B3)}$$

with the phase angle ξ defined by

$$\cos(\xi) = \cos(\theta_s)\cos(\theta_v) + \sin(\theta_s)\sin(\theta_v)\cos(\phi). \quad \text{(B4)}$$

The explicit formulas for the surface parameters k_0, k_1, and k_2 can be found in the Roujean *et al*. study [17] or the 6S manual [5].

Appendix C. Ocean Surface Model

The reflectance ρ_{os} of an ocean surface is calculated for a given set of geometrical conditions and a specified wavelength λ as the sum of three components [22]:

$$\rho_{os}(\theta_s,\ \theta_v,\ \phi,\ \lambda) = \rho_{wc}(\lambda) + \{1 - W\}\cdot\rho_{gl}(\theta_s,\ \theta_v,\ \phi,\ \lambda) + \{1 - \rho_{wc}(\lambda)\}\cdot\rho_{sw}(\theta_s,\ \theta_v,\ \phi,\ \lambda), \quad \text{(C1)}$$

where $\rho_{wc}(\lambda)$ is the reflectance due to whitecaps, $\rho_{gl}(\theta_s, \theta_v, \phi, \lambda)$ is the specular reflectance at the ocean surface, $\rho_{sw}(\theta_s, \theta_v, \phi, \lambda)$ is the scattered reflectance emerging from sea water, and W is the relative area covered with whitecaps, expressed from the wind speed w_s as $W = 2.9510^{-6}\, w_s^{3.52}$ for water temperatures greater than 14 °C [27].

The first term of Eq. (C1) is defined as the weighted product of the fraction of ocean surface covered with whitecaps and the reflectance of whitecaps $\rho_f(\lambda)$:

$$\rho_{wc}(\lambda) = W\cdot f_{ef}\cdot\rho_f(\lambda), \quad \text{(C2)}$$

where $f_{ef} = 0.4 \pm 0.2$ is the efficiency factor accounting for the increase in the size of an individual whitecap with age [22].

The calculation of the second term of Eq. (C1) depends on Fresnel's reflection coefficient $R(n, \theta_s, \theta_v, \phi, \lambda)$ as

$$\rho_{gl}(\theta_s,\ \theta_v,\ \phi,\ \lambda) = \frac{\pi P(Z_x',\ Z_y')R(n,\ \theta_s,\ \theta_v,\ \phi,\ \lambda)}{4\cos(\theta_s)\cos(\theta_v)\cos^4(\beta)}, \quad \text{(C3)}$$

where n is the complex refractive index of sea water, $P(Z_x', Z_y')$ is the slope distribution, Z_x' and Z_y' are the slope components, and β is the tilt angle [23–26].

The third term of Eq. (C1) is the reflectance observed just above the sea surface (level 0^+). It can be related to the ratio R_w of upwelling to downwelling radiance just below the sea surface (level 0^-) as [23–25,28]

$$\rho_{sw}(\theta_s,\ \theta_v,\ \phi,\ \lambda) = \frac{1}{n^2}\frac{R_w(\lambda)\cdot t_d(\theta_s)\cdot t_u(\theta_v)}{1 - a\cdot R_w(\lambda)}, \quad \text{(C4)}$$

where $t_d(\theta_s)$ and $t_u(\theta_v)$ are the transmittances for downwelling and upwelling radiances, calculated on the basis of the Fresnel reflectance coefficient for the air–water interface, and $a = 0.485$.

A more detailed description can be found in the 6S manual [5].

The authors thank P. Farris for help with the preparation of this manuscript. They also thank F.-M. Bréon for providing the Monte Carlo code, A. I. Lyapustin for providing the SHARM code, and the anonymous reviewers for their helpful comments. This work was supported by NASA contract NNG04HZ17C.

References

1. S. Y. Kotchenova, E. F. Vermote, R. Matarrese, and F. Klemm, "Validation of a vector version of the 6S radiative transfer code for atmospheric correction of satellite data. Part I: path radiance," Appl. Opt. **45,** 6762–6774 (2006).
2. E. F. Vermote, N. Z. El Saleous, and C. O. Justice, "Atmospheric correction of MODIS data in the visible to middle infrared: first results," Remote Sens. Environ. **83,** 97–111 (2002).
3. J. L. Deuzé, M. Herman, and R. Santer, "Fourier series expansion of the transfer equation in the atmosphere-ocean system," J. Quant. Spectrosc. Radiat. Transfer **41,** 483–494 (1989).
4. K.-N. Liou, *An Introduction to Atmospheric Radiation* (Academic, 1980).
5. E. F. Vermote, D. Tanré, J. L. Deuzé, M. Herman, J. J. Morcrette, S. Y. Kotchenova, and T. Miura, *Second Simulation of the Satellite Signal in the Solar Spectrum (6S), 6S User Guide Version 3* (November, 2006), http://www.6s.ltdri.org.
6. F. F. Evans and G. L. Stephens, "A new polarized atmospheric radiative transfer model," J. Quant. Spectrosc. Radiat. Transfer **5,** 413–423 (1991).
7. J. V. Dave and J. Gazdag, "A modified Fourier transform method for multiple scattering calculation in a plane-parallel Mie atmosphere," Appl. Opt. **9,** 1457–1465 (1970).
8. J. V. Dave, "Coefficients of the Legendre and Fourier series for the scattering functions of spherical particles," Appl. Opt. **9,** 1888–1896 (1970).
9. A. I. Lyapustin, "Radiative transfer code SHARM for atmospheric and terrestrial application," Appl. Opt. **44,** 7764–7772 (2005).
10. M. I. Mishchenko, A. A. Lacis, and L. D. Travis, "Errors induced by the neglect of polarization in radiance calculations for Rayleigh-scattering atmospheres," J. Quant. Spectrosc. Radiat. Transfer **51,** 491–510 (1994).
11. A. A. Lacis, J. Chowdhary, M. I. Mishchenko, and B. Cairns,

"Modeling errors in diffuse-sky radiation: Vector vs. scalar treatment," J. Geophys. Res. **25,** 135–138 (1998).
12. M. I. Mishchenko and L. D. Travis, "Satellite retrieval of aerosol properties over the ocean using polarization as well as intensity of reflected sunlight," J. Geophys. Res. **102,** 16989–17013 (1997).
13. A. Lyapustin, "Radiative transfer code SHARM-3D for radiance simulations over a non-Lambertian nonhomogeneous surface: intercomparison study," Appl. Opt. **41,** 5607–5615 (2002).
14. H. Rahman, B. Pinty, and M. M. Verstraete, "Coupled surface-atmosphere reflectance (CSAR) model. 2. Semiempirical surface model usable with NOAA Advanced Very High Resolution Radiometer Data," J. Geophys. Res. **98,** 20791–20801 (1993).
15. K. L. Coulson, J. V. Dave, and Z. Sekera, *Tables Related to Radiation Emerging from a Planetary Atmosphere with Rayleigh Scattering* (University of California Press, 1960).
16. F.-M. Bréon, "Reflectance of broken cloud fields: simulation and parameterization," J. Atmos. Sci. **49,** 1221–1232 (1992).
17. J.-L. Roujean, M. Leroy, and P. Y. Deschamps, "A bidirectional reflectance model of the Earth's surface for the correction of remote sensing data," J. Geophys. Res. **97,** 20455–20468 (1992).
18. O. Engelsen, B. Pinty, M. M. Verstraete, and J. V. Martonchik, *Parametric Bidirectional Reflectance Factor Models: Evaluation, Improvements and Applications,* Eur. Rep. 16426 EN (Space Appl. Inst., Ispra, Italy, 1996).
19. W. Lucht, C. B. Schaaf, and A. H. Strahler, "An algorithm for the retrieval of albedo from space using semiempirical BRDF models," IEEE Trans. Geosci. Remote Sens. **38,** 977–998 (2000).
20. C. B. Schaaf, F. Gao, A. H. Strahler, W. Lucht, X. Li, T. Tsang, N. C. Strugnell, X. Zhang, Y. Jin, J.-P. Muller, P. Lewis, M. Bamsley, P. Hobson, M. Disney, G. Roberts, M. Dunderdale, C. Doll, R. P. d'Entremont, B. Hu, S. Liang, J. L. Privette, and D. Roy, "First operational BRDF, albedo nadir reflectance products from MODIS," Remote Sens. Environ. **83,** 135–148 (2002).
21. D. S. Kimes, W. W. Newcomb, R. F. Nelson, and J. B. Schutt, "Directional reflectance distributions of a hardwood and a pine forest canopy," IEEE Trans. Geosci. Remote Sens. **24,** 281–293 (1986).
22. P. Koepke, "Effective reflectance of oceanic whitecaps," Appl. Opt. **23,** 1816–1824 (1984).
23. C. Cox and W. Munk, "Measurement of the roughness of the sea surface from photographs of the sun's glitter," J. Opt. Soc. Am. **44,** 838–850 (1954).
24. C. Cox and W. Munk, "Statistics of the sea surface derived from sun glitter," J. Mar. Res. **13,** 198–227 (1954).
25. C. Cox and W. Munk, "Some problems in optical oceanography," J. Mar. Res. **14,** 63–78 (1955).
26. M. Born and E. Wolf, *Principles of Optics,* 5th ed. (Pergamon, 1975).
27. E. C. Monahan and I. O'Muircheartaigh, "Optimal power-law description of oceanic whitecap dependence on wind speed," J. Phys. Oceanogr. **10,** 2094–2099 (1980).
28. A. Morel, "Optical modeling of the upper ocean in relation to its biogenous matter content (Case I Waters)," J. Geophys. Res. **93,** 10479–10768 (1988).
29. L. D. Talley and G. C. Johnson, "Deep, zonal subequatorial currents," Science **263,** 1125–1128 (1994).
30. C. C. Trees, D. K. Clark, R. R. Bidigare, M. E. Ondrusek, and J. L. Mueller, "Accessory pigments versus chlorophyll a concentrations within the Euphotic Zone: A ubiquitous relationship," Limnol. Oceanogr. **45,** 1130–1143 (2000).
31. Salt Concentration, www.nas.nasa.gov/News/Archive/2006/08-30-06.html.
32. E. Vermote and D. Tanré, "Analytical expressions for radiative properties of planar Rayleigh scattering media, including polarization contributions," J. Quant. Spectrosc. Radiat. Transfer **47,** 305–314 (1992).
33. B. M. Herman, T. R. Caudill, D. E. Flittner, K. J. Thome, and A. Ben-David, "Comparison of the Gauss–Seidel spherical polarized radiative transfer code with other radiative transfer codes," Appl. Opt. **34,** 4563–4572 (1995).
34. K. Masuda, "Infrared sea surface emissivity including multiple reflection effect for isotropic Gaussian slope distribution model," Remote Sens. Environ. **103,** 488–496 (2006).
35. G. A. d'Almeida, P. Koepke, and E. P. Shettle, *Atmospheric Aerosols: Global Climatology and Radiative Characteristics* (Deepak Publishing, 1991).
36. Midway Islands, https://www.cia.gov/cia/publications/factbook/geos/um.html.